

¹ Chapter 1

² Diamond irradiation study

³ The aim of the study in this chapter is to find the operational limitations of diamond
⁴ detectors for spectroscopy and tracking applications. The chapter contains the mea-
⁵ surement results of data taken with diamond sensors. First the measurement setup
⁶ is described in section 1.1. Then the measured particle spectra are shown in 1.2.
⁷ This is followed by a study of effects of the irradiation damage on the electrical signal
⁸ of the diamond detector. The last section shows the results of the measurements
⁹ of irradiated diamond samples at cryogenic temperatures. The studies compare the
¹⁰ experimentally acquired data with the theory from the previous chapter and define
¹¹ limitations of the diamond detectors in terms of radiation and temperature.

¹² Diamond sensors are mainly used for two types of measurements: particle counting
¹³ and spectroscopy. The first type of measurements depends on the sensor efficiency –
¹⁴ its ability to detect all or at least a known percentage of incident particles. The energy
¹⁵ of the particles is not so important; what bears the information is the rate and the
¹⁶ spatial distribution. Here the particles do not necessarily stop in the bulk, but rather
¹⁷ continue their way. In spectroscopy, on the other hand, the particles stop within the
¹⁸ sensor, depositing all their energy. This energy is then measured by collecting the
¹⁹ freed charge carriers. The goal of the experiments described in this chapter is to:

- ²⁰ 1. Quantify the efficiency of the sCVD diamond in counting mode,
- ²¹ 2. Quantify the degradation of the efficiency as a function of the received radiation
dose,
- ²³ 3. Quantify the macroscopic effects on charge carrier behaviour as a function of
the received radiation dose and
- ²⁵ 4. Define limitations for use in spectroscopy.

²⁶ The results discussed here show that there are several limitations for using diamond as
²⁷ a radiation detector. All of them need to be taken into account when designing a new
²⁸ measurement device. The irradiation study allows for an estimation of the lifetime of
²⁹ the detector and a prediction of the longterm signal degradation as a function of the

1.1. MEASUREMENT SETUP

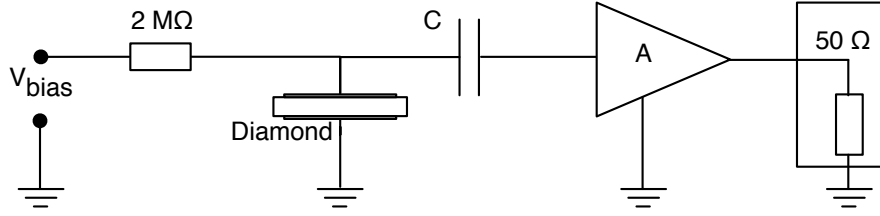


Figure 1.1: Diagram of a diamond detector readout chain.

30 received radiation dose. The result of the study is a correction factor, which can be
31 applied during data analysis to ensure that the analysis results are stable despite the
32 detector degradation.

33 1.1 Measurement setup

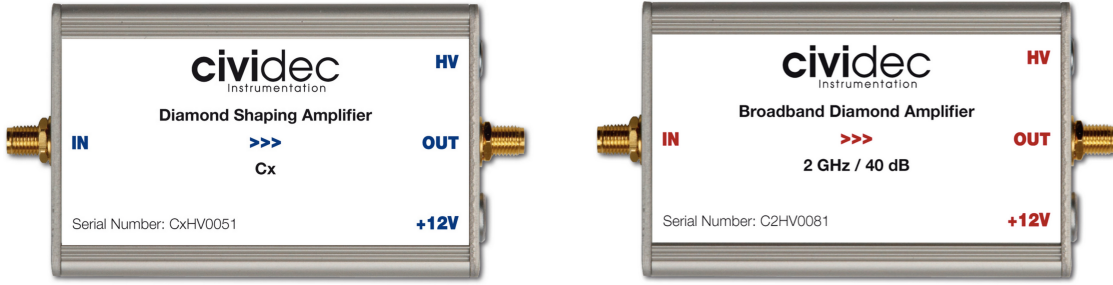
34 The first step of designing a measurement setup is to define the measurement conditions,
35 such as the temperature, the type of radiation and its flux. The second step is
36 to ensure that the setup is insensitive to external electromagnetic interferences and
37 that it minimises electrical noise in the system. The setup needs to be calibrated
38 before use.

39 Shielding has to be applied wherever possible. For instance, aluminium foil can
40 be wrapped around the exposed parts of the system to shield them from external
41 radio-frequency (RF) interferences. In addition, the sensors have to be covered to
42 prevent the exposure to light. The incident photons may deposit enough energy to
43 increase the leakage current of the detector, which produces unwanted results.

44 The measurements using diamond that are explained in these chapters have been
45 carried out using several measurement setups, but they are all similar in terms of
46 the electrical signal chain. The measurement chain consists of three main parts: a
47 diamond sensor, a signal preamplifier and a readout device, as seen in figure 1.1. The
48 signals propagating along the analogue chain are fast – in the GHz bandwidth range –
49 and with low amplitudes – of the order of tens of μV . This gives rise to the importance
50 of RF shielding. Also, the connection between the carrier and the preamplifier has
51 to be as short as possible to avoid capacitive signal losses in the transmission line.
52 Finally, the system needs to be grounded properly.

53 1.1.1 Preamplifiers

54 Two preamplifiers are used for the measurements, one sensitive to charge and the
55 other to current. *CIVIDEC Cx* (figure 1.2a) is a charge sensitive amplifier. Its high
56 SNR is achieved due to a low equivalent noise charge of 300 e^- with an additional
57 30 e^- per each pF of the sensor capacitance. A reported gain of $\sim 12 \text{ mV/fC}$ makes



(a) Cx charge sensitive preamplifier.

(b) C2 fast charge preamplifier.

Figure 1.2: Amplifiers used for the charge and current measurements.

58 it a good choice for spectroscopic measurements with diamond sensors. *CIVIDEC*
 59 *C2* (figure 1.2b) is a fast current preamplifier with a 2 GHz bandwidth limit. It is
 60 used for TCT measurements because of its fast response and a good SNR. Both are
 61 embedded in an RF-tight aluminium box to reduce the noise pickup. Both have an
 62 AC coupled input and an output with a 50Ω termination.

63 A 2 GHz bandwidth limit defines the minimum rising time equal to $t_r \simeq \frac{0.34}{BW} =$
 64 $\frac{0.34}{2 \times 10^9} = 170 \text{ ps}$, therefore the system with a CIVIDEC C2 amplifier is capable of
 65 measuring pulses with a minimum FWHM $\simeq 170 \text{ ps}$. The initial peak in the α pulse
 66 has a lower FWHM; for example, if a charge carrier travelling through the bulk takes
 67 $t_1 \sim 6 \text{ ns}$ to reach the electrode on the opposite side ($d_1 \sim 500 \mu\text{m}$), the carrier with
 68 the opposite charge and a shorter path to the closer electrode – max. $d_2 \sim 10 \mu\text{m}$ –
 69 only takes $t_2 \sim \frac{d_2}{d_1} t_1 = 120 \text{ ps}$. A drift time this short induces a current pulse that is
 70 too narrow for the system to observe.

71 Calibration

72 The amplifiers have to be calibrated before use to determine their gain. Both are
 73 calibrated using a square signal generator with a known amplitude step of $U_{\text{in}} =$
 74 $(252 \pm 5) \text{ mV}$. A 2 GHz oscilloscope with a 10 GS/s sampling rate is used to carry
 75 out the calibration.

76 **Cx charge sensitive amplifier** calibration necessitates an injection of a well known
 77 charge. Therefore the signal from a pulse generator is routed through a capacitor with
 78 a calibration capacitance $C_{\text{cal}} = (0.717 \pm 0.014) \text{ pF}$ and then to the input of the am-
 79 plifier. The pulse area behind the capacitor is $a_{\text{cal}} = (5.0 \pm 0.5) \text{ pVs}$, with the signal
 80 amplitude on the output amounting to $U_{C_x} = (1.95 \pm 0.05) \text{ V}$. The input voltage step
 81 combined with the calibration capacitance yields a calibration charge

$$Q_{\text{cal}} = C_{\text{cal}} \cdot U_{\text{in}} = (181 \pm 5) \text{ fC}. \quad (1.1)$$

82 The gain of the Cx amplifier when comparing the integrated input charge to the

1.1. MEASUREMENT SETUP

83 output amplitude is

$$A_{Cx}^Q = \frac{U_{Cx}}{Q_{\text{cal}}} = (9.3 \pm 0.4) \text{ mV/fC} \quad (1.2)$$

84 whereas the factor between the area of the input current pulse and the output am-
85 plitude is

$$A_{Cx}^a = \frac{U_{Cx}}{a_{\text{cal}}} = (390 \pm 40) \text{ mV/pVs.} \quad (1.3)$$

86 The area-based amplification factor A_{Cx}^a can be used as an estimate for the integrated
87 charge of a current pulse. However, it has a higher uncertainty ($\sim 10\%$) than
88 the amplitude-based factor A_{Cx}^Q ($\sim 4\%$) due to the measurement limitations of the
89 oscilloscope.

90 **C2 current amplifier** calibration only requires the measurement of the amplitude
91 gain. To keep the output signal amplitude within the ± 1 V linear range of the
92 amplifier, the input signal amplitude has to be minimised. The signal from the
93 generator is therefore routed through a 36 dB attenuator to decrease its amplitude to
94 $U_{\text{inAtt}} = (3.95 \pm 0.05)$ mV. Two amplifiers with different gains have been measured,
95 because both are used for the measurements. The output of the first amplifier amounts
96 to $U_{C2-1} = (860 \pm 5)$ mV. This yields the amplification gain

$$A_{C2-1} = \frac{U_{\text{inAtt}}}{U_{C2-1}} = (217 \pm 3). \quad (1.4)$$

97 The second amplifier has the output equal to $U_{C2-2} = (632 \pm 5)$ mV with the resulting
98 gain of $A_{C2-2} = (152 \pm 3)$.

99 1.1.2 Diamond samples

100 Detector-grade diamonds are very difficult to produce. The major challenge is to
101 ensure a high enough purity of the lattice. The sensor samples used for these studies
102 have been acquired from Element Six (E6) [2]. They all have the same standard
103 dimensions. sCVD diamonds with dimensions $4.7 \times 4.7 \text{ mm}^2$ are already sufficiently
104 large for most of the beam monitoring applications and still affordable. One sample
105 with dimensions of $5.6 \times 5.3 \text{ mm}^2$ produced by IIa Singapore [3] has also been char-
106 acterised at CERN [19]. The target thickness for all samples is $500 \mu\text{m}$. Diamonds
107 this thick yield a high enough signal-to-noise ratio for MIPs to be measured by the
108 available electronics. Table 1.1 shows all the samples used for this study. Two of
109 them are measured before and after irradiation and then compared. Irradiation doses
110 for damaging the material need to be high – above 10^{12} particles per cm^2 to be able
111 to observe a significant change in behaviour of a diamond sensor.

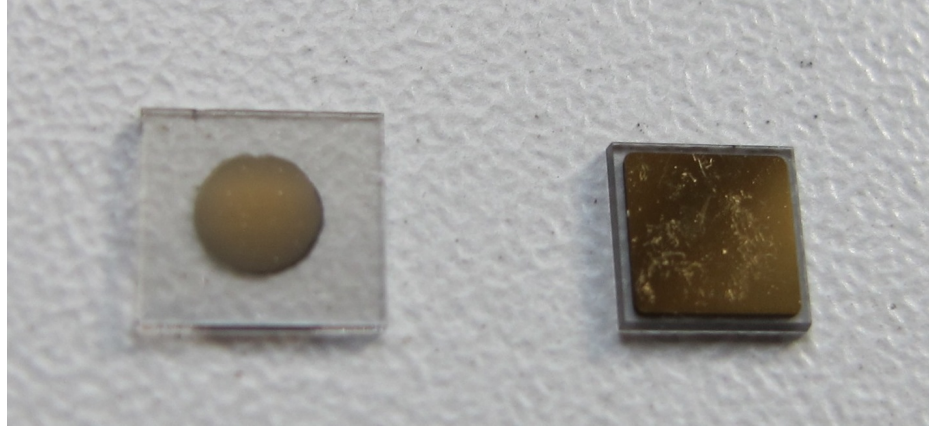


Figure 1.3: Two scCVD diamond samples: A IIa 1scdhq (left) and an E6 S37 (right).

	Name	Type	Producer	Dimensions [mm ²]	Thickness [μm]	Electrode	Irradiated
	S37	sCVD	E6	4.7 × 4.7	548	Cr/Au	no
	S50	sCVD	E6	4.7 × 4.7	537	Cr/Au	no
113	S52	sCVD	DDL	4.7 × 4.7	515	DLC/Pt/Au	$3.63 \times 10^{14} \frac{\pi}{cm^2}$
	S79	sCVD	E6	4.7 × 4.7	529	Cr/Au	$1 \times 10^{14} \frac{\pi}{cm^2}$
	ELSC	sCVD	E6	4.7 × 4.7	491	Cr/Au	no
	1scdhq	sCVD	IIa	5.6 × 5.3	460	Cr/Au	no

Table 1.1: Diamond sensor samples used.

115 The diamond samples have quoted impurity densities of $\leq 2 \times 10^{14} \text{ cm}^{-3}$ and ni-
 116 trogen incorporation of $\leq 10^{-9}$. The electrodes were added by various companies and
 117 institutes. For instance, S52 was metallised by a company DDL (now defunct) while
 118 the Physics Department of the University of Firenze, Italy metallised the S79. There
 119 are also several techniques for producing the electrodes. The DDL contacts consist
 120 of three layers: DLC (diamond-like carbon)/Pt/Au with 4/10/200 nm thicknesses,
 121 respectively. The metallisation for S79, on the other hand, is made up of Cr/Au
 122 with a total thickness of ~ 400 nm. The area coverage also differs from sample to
 123 sample. Diamonds must not be metallised until the very edge as the proximity of
 124 contacts with a high potential may lead to sparking. However, the areas not covered
 125 by the metallisation are less efficient because the fringe fields at the edges are not
 126 as strong as in between the electrodes. This effectively reduces the sensitive area of
 127 the sensors. In the diamonds used here the effective area is anywhere from 9 mm² to
 128 18 mm². The leakage current is below 1 nA, but increases for the irradiated samples.
 129 The capacitance is of the order of (2.0 ± 0.3) pF.

130 1.1.3 Readout devices

131 Electrical signals in diamond detectors are in the GHz frequency range. To preserve
 132 the information in the signals, the readout device with a high bandwidth limit must

1.1. MEASUREMENT SETUP

be used. For instance, a 250 MHz limit is enough for the spectroscopic measurements with the Cx charge amplifier, but might be insufficient for the current measurements with the C2 amplifier.

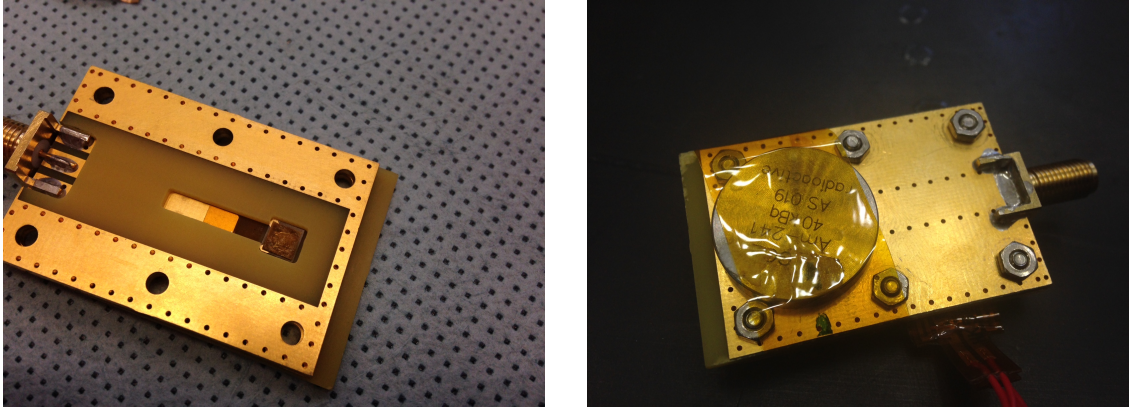
Two devices are used take data shown in this chapter. The first choice is a 2 GHz LeCroy WaveRunner 204MXi-A. This specific model has a sufficiently high bandwidth limit for the fast current preamplifier signals. It offers a reliable solution for analogue signal readout of limited amounts of data. However, its slow acquisition speed is a bottleneck in a test beam experiment. Its initial 100 Hz readout rate decreases to a mere 20 Hz within 20 minutes, because every single trigger is saved as a separate file and the Windows operating system is not capable of handling 10000+ files in a single directory easily. This is why it has been exchanged with a DRS4 [1], an analogue readout device developed by PSI, Switzerland. This compact device is capable of recording up to four waveforms at a time at a steady rate of up to 500 Hz. Its 700 MHz bandwidth limitation is sufficient for the signal from the charge amplifier.

1.1.4 Setup for the β detection efficiency study

The efficiency study of the diamond sensors has been carried out at CERN in the North Hall test beam facility. There a straight high-energy particle beam of 120 GeV π is provided to the users to calibrate their detectors. The beam has a transverse spread of $\sigma = 10$ mm in both axes. The particle rate is of the order of $10^4 \pi \text{ cm}^{-2} \text{ s}^{-1}$. A diamond sensor embedded in a printed circuit board (PCB) carrier has been placed in the beam spot perpendicular to the beam and connected via an SMA connector directly to a charge amplifier. The amplified signal is read out using a LeCroy oscilloscope and a DRS4 analogue readout system. A computer is used as a controller and data storage for the readout device. A beam telescope is used as a reference detector. It is a device that helps to cross-check the measurements of the devices under test (DUTs) and to carry out spatially resolved studies on the DUTs. It consists of several pixellated sensor planes placed in series, which can track a particle's trajectory with a precision of a few μm . The sensor planes are positioned in front of the DUT and behind it. Then the beam telescope acts as a trigger system – it triggers the readout of both the telescope data and DUT data when both the planes in front and behind the DUT record a hit by an incident particle. A particle detected by all the planes within the DUT window and the DUT itself counts towards its efficiency whereas a hit missed by the DUT means that the DUT is not 100 % efficient. To discard the hits that miss the DUT completely, a region of interest (ROI) can be chosen in the beam telescope planes. The equation for calculating the sensor efficiency is therefore

$$\epsilon = \frac{N_{\text{DUT}} \wedge N_{\text{telescope}}}{N_{\text{telescope}}} \quad (1.5)$$

for an ROI smaller than the sensitive region of the diamond.



(a) PCB carrier with an embedded diamond sample.
 (b) Radioactive source over the carrier.

Figure 1.4: Positioning of the α -source on top of the sensor carrier.

¹⁶⁹ 1.1.5 Room temperature α -TCT setup

¹⁷⁰ This TCT study is a follow-up of an extensive diamond TCT study at cryogenic
¹⁷¹ temperatures [13]. The room-temperature TCT measurements have been carried
¹⁷² out in the laboratory. The setup consists of a diamond sensor embedded in a PCB
¹⁷³ carrier, a current amplifier and an oscilloscope. To measure α particles, their energy
¹⁷⁴ loss during their trajectory has to be minimised. Therefore the diamond is placed
¹⁷⁵ inside a vacuum chamber. The chamber is a steel tube with a diameter of 5 cm.
¹⁷⁶ On one side it is connected to a vacuum pump via a steel hose. A feedthrough with
¹⁷⁷ an SMA connector is placed on the other side. A CIVIDEC C2 current amplifier is
¹⁷⁸ connected directly onto the feedthrough. The amplified output is connected to the
¹⁷⁹ oscilloscope via an SMA cable. An ^{241}Am source with a diameter of 2 cm and a
¹⁸⁰ height of 0.5 cm is fixed onto the sensor carrier (figure 1.4a, figure 1.4b). Then the
¹⁸¹ carrier is inserted in the chamber and fixed in place using an air-tight clamp. The
¹⁸² pump can then be switched on. It is capable of providing the inside pressure as low
¹⁸³ as 10^{-4} mbar after approximately one hour of operation.

¹⁸⁴ 1.1.6 Cryogenic α -TCT setup

¹⁸⁵ The experiment at cryogenic temperatures has been carried out at the Central Cryo-
¹⁸⁶ genic Laboratory at CERN. The room-temperature TCT setup has to be modified to
¹⁸⁷ allow for measurements at temperatures as low as 2 K. It consists of three parts:

- ¹⁸⁸ 1. a cryostat – a thermally insulated cylinder containing liquid helium,
- ¹⁸⁹ 2. an inlet – an air-tight mechanical tube with valves and feedthroughs at the top
¹⁹⁰ that is lowered in the liquid helium and

1.2. CHARGED PARTICLE PULSES AND SPECTRA

191 3. the diamond sample embedded in a PCB carrier with a fitted temperature
192 sensor, a heater and cables leading to the feedthroughs.

193 The setup is described in detail in [13].

194 When the diamond sample is placed in the PCB carrier and the ^{241}Am source
195 is in place, the inlet is sealed and lowered in the empty cryostat. Then the inside
196 volume of the inlet is evacuated down to 10^{-5} mbar while the liquid helium is flowing
197 into the cryostat. To improve the thermal contact between the diamond and the
198 coolant, a small amount of helium gas is added inside the evacuated inlet, setting
199 the vacuum to around 10^{-3} mbar. This value changes with time, because the gas
200 condenses on the walls of the inlet, reducing the number of floating particles. For this
201 reason the helium gas has to be added on an irregular basis. Every addition causes a
202 significant undershoot of the sample temperature, which has to be corrected for using
203 a heater placed on the back of the PCB carrier. Also, the added gas deteriorates the
204 vacuum inside the inlet. Furthermore, at approximately 60 K the helium gas has to
205 be evacuated from the inlet to avoid a potential explosion due to the expansion of
206 the gas with temperature.

207 When the sample is cooled to 4.2 K, the minimum temperature achievable by
208 means of liquid helium without over-pressurising it, the measurements can begin. A
209 temperature sensor placed on the back of the PCB carrier is used to measure the
210 temperature of the sample. After every temperature data point, the current through
211 the heater placed in the PCB next to the diamond sample is increased, increasing the
212 sample. The initial temperature time constant of the order of tenths of seconds at low
213 temperatures increases with temperature. Even more so when helium is evacuated
214 from the inlet at 60 K, removing the thermal bridge between the wall of the inlet and
215 the diamond sample. At the room temperature (RT), the time constant is already of
216 the order of minutes.

217 1.2 Charged particle pulses and spectra

218 In previous chapter the ionisation profiles for different types of radiation were dis-
219 cussed. β radiation induces a triangular electric pulse whereas α radiation induces
220 a rectangular one. However, their amplitude, width and rise/fall time depend heav-
221 ily on the type of interaction with the diamond, the purity of the diamond and the
222 bandwidth of the amplifier and the oscilloscope. This section shows the signal pulses
223 of α , β and γ radiation with their respective energy distributions for the case of a
224 diamond detector.

225 Figure 1.5 shows a set of pulses and an averaged waveform for 5.5 MeV α , 2.3 MeV
226 β and 1.3 MeV γ radiation using an ^{241}Am , a ^{90}Sr and a ^{60}Co source, respectively.
227 The particles are measured with the non-irradiated sCVD diamond S37. α particles
228 always produce the same signal pulse, but with a high noise RMS. The averaging
229 suppresses the noise while retaining most the information. It does, however, smear

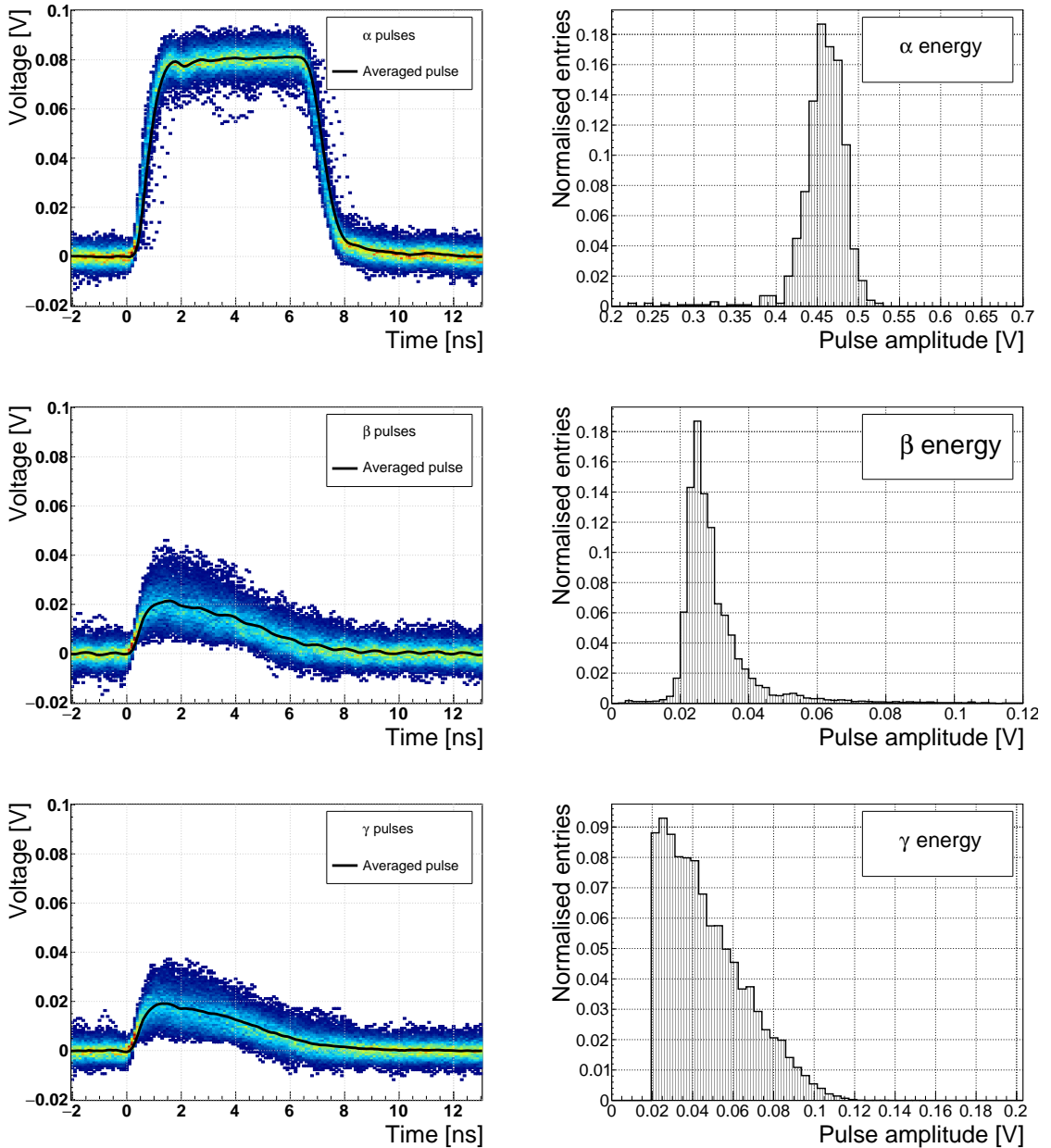


Figure 1.5: Superimposed and averaged pulses (left figures, current amplifier) and distributions of deposited energy (right figures, charge amplifier) for three types of radiation. Note the scale on the X axis of the distributions.

the rising and falling edge, increasing the rising and falling time. The t_r is now of the order of 0.5 ns. Both β and γ pulses look similar - triangular and with a wide range of amplitudes. Here the pulse count is low, so the pulses with a high amplitude are not recorded. A trigger would need to be set very high to “catch” them with the oscilloscope.

²³⁵ **1.3 Radiation limitations**

²³⁶ This section quantifies the decrease in charge collection efficiency as well as the effects
²³⁷ on long-term measurement stability in irradiated sCVD diamonds.

²³⁸ **1.3.1 Irradiation study**

²³⁹ This subsection contains a study of the effects of 300 MeV pion (π) irradiation
²⁴⁰ on the charge collection efficiency of sCVD diamond detectors. To carry out this
²⁴¹ study, two diamond samples were irradiated to doses of $1 \times 10^{14} \pi \text{ cm}^{-2}$ (S79) and to
²⁴² $3.63 \times 10^{14} \pi \text{ cm}^{-2}$ (S52). A test beam campaign was carried out to observe the charge
²⁴³ collection efficiency at different bias voltage settings. The efficiency values acquired
²⁴⁴ are used to determine the effective drop in efficiency as a function of the received
²⁴⁵ radiation dose. This is to test if the collected charge Q is inversely proportional to
²⁴⁶ the received dose Φ . A procedure defined by a collaboration researching diamond be-
²⁴⁷ haviour RD42 has been applied to the measured values to extract the damage factor
²⁴⁸ (described in ??).

²⁴⁹ The following subsection contains measurements and results of a long-term stabil-
²⁵⁰ ity study using α and β particles. In particular, the charge collection efficiency with
²⁵¹ β and α radiation as a function of time is measured. To investigate this effect on the
²⁵² scale of charge carriers, the change of TCT (transient current technique) pulses with
²⁵³ time is observed. Finally, a procedure that improves the pulse shape and with it the
²⁵⁴ charge collection is proposed.

²⁵⁵ **Irradiation with a 300 MeV π beam**

²⁵⁶ The samples were irradiated at the Paul Scherrer Institute (PSI) [4] by means of a
²⁵⁷ beam of pions with an energy of 300 MeV (kinetic energy 191.31 MeV) and with a flux
²⁵⁸ of up to $1.5 \times 10^{14} \pi \text{ cm}^{-2}$ per day. The system has a 10 % uncertainty on the beam
²⁵⁹ energy. Looking at the pion damage curve in figure ??, $\pi_{300 \text{ MeV}}$ point (191 MeV
²⁶⁰ kinetic energy) sits on a steep section of the DPA curve. This means that a deviation
²⁶¹ in beam energy can have a significant effect on the damage in the sensor. In addition,
²⁶² their quoted uncertainty on the measurement of the delivered dose is $\pm 20 \%$.

²⁶³ Two diamond samples, S52 and S79, were put in the $\pi_{300 \text{ MeV}}$ beam in the 2014
²⁶⁴ PSI irradiation campaign; S52 to $(1 \pm 0.21) \times 10^{14} \pi \text{ cm}^{-2}$ and S79 to $(3.63 \pm 0.77) \times$
²⁶⁵ $10^{14} \pi \text{ cm}^{-2}$. During the process, the gold electrodes got slightly activated, but the
²⁶⁶ activation decayed in two weeks.

²⁶⁷ **300 MeV π radiation damage factor**

²⁶⁸ Three diamonds – non-irradiated S37 and irradiated S52 and S79 – were tested in a
²⁶⁹ $\pi_{120 \text{ GeV}}$ test beam in the SPS North Experimental Area at CERN [8] before and after

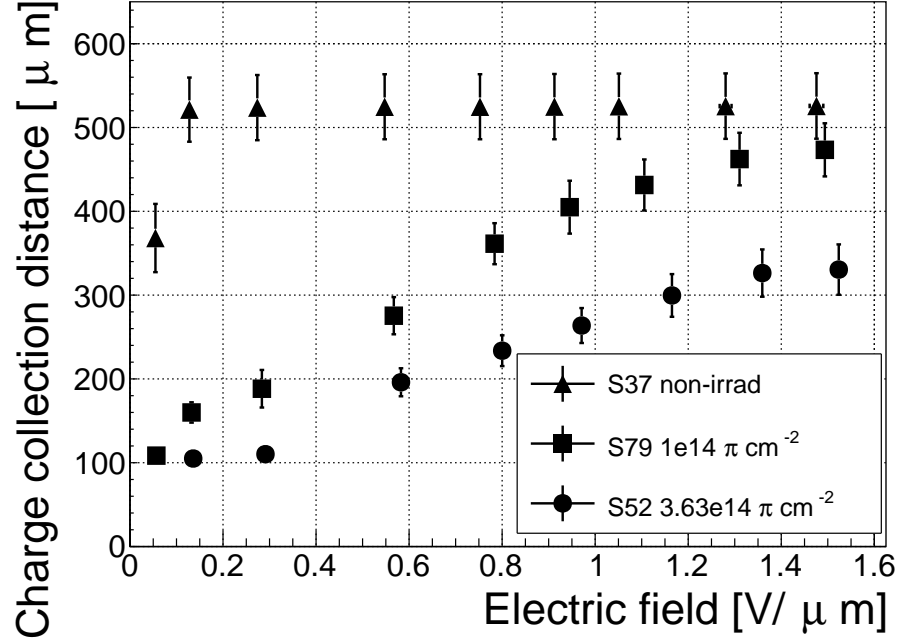


Figure 1.6: The figure shows the CCD for S37, S79 and S52 at a range of bias voltage settings.

irradiation. The goal was to estimate the charge collection efficiency and charge collection distance as a function of irradiation dose. The samples were primed (pumped) prior to data taking using a ^{90}Sr radioactive source. The data were then taken at a range of bias voltages ranging from 30 V to 900 V, yielding between $0.06 \text{ V}/\mu\text{m}$ and $1.8 \text{ V}/\mu\text{m}$ electrical field in the bulk. Every data point contained approximately 5×10^4 measured particles. The charge deposited by the particles was measured using a CIVIDEC Cx charge preamplifier.

As expected, the integrated amplitude spectrum is a Landau distribution. Its most probable value (MPV) is used to calculate the most probable collected charge Q_i :

$$Q_i [\text{e}^-] = \frac{1}{1.6 \times 10^{-19}} Q_i [\text{C}] = 6241 \cdot Q_i [\text{fC}] = 6241 \cdot \frac{\text{MPV} [\text{mV}]}{A [\frac{\text{mV}}{\text{fC}}]}, \quad (1.6)$$

where $A = 9.3 \text{ mV/fC}$ is the preamplifier gain factor and $1 \text{ e}^- = 1.6 \times 10^{-19} \text{ C}$.

The CCD for the three measured samples at a bias voltages ranging from $0.2 - 1.6 \text{ V } \mu\text{m}^{-1}$ calculated using equation ?? is shown in figure 1.6. S37 exhibits a full collection distance already at $0.4 \text{ V } \mu\text{m}^{-1}$ whereas the irradiated samples have a more gentle increase of CCD with increasing bias voltage. It is evident that at $1 \text{ V } \mu\text{m}^{-1}$ the maximum CCD has not been reached in the case of S79 and S52. Nevertheless, to compare the measured data point with those provided by RD42, the CCD at $1 \text{ V } \mu\text{m}^{-1}$ has to be taken.

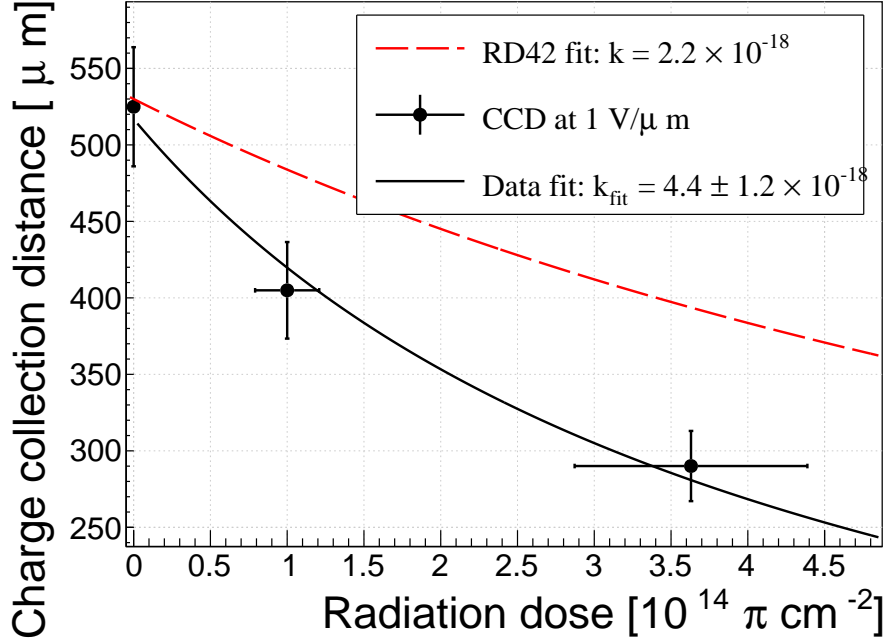


Figure 1.7: The charge collection distance at $1 \text{ V}/\mu\text{m}$ bias voltage for the three diamond samples is plotted as a function of the received radiation dose. It is compared to the RD42 data for pion irradiation. The data points are about 15–25 % lower than expected from the RD42 data [17].

288 The data points with the maximum CCD obtained in the test beam measurements
 289 are plotted against received radiation dose in figure 1.7. Equation ?? is fitted to the
 290 data points and a damage factor $k_\lambda = (4.4 \pm 1.2) \times 10^{-18} \mu\text{m}^{-1} \text{ cm}^{-2}$ is obtained. The
 291 value is for a factor of two higher than the damage factor obtained by RD42. This
 292 could be due to an insufficient priming time ahead of the measurement. In addition,
 293 the diamond samples have not been polished and re-metallised after irradiation, as
 294 is the case for the RD42. Also, with only two samples measured, the statistical
 295 uncertainty is high. Nevertheless, it can be concluded that the 300 MeV pions damage
 296 the diamond bulk significantly more than the 24 GeV protons.

297 **1.3.2 Long-term measurement stability**

298 An important requirement for particle detectors is a stable performance over long
 299 periods of time. For instance, the charge collection for a defined radiation type and
 300 quantity must not change over time or has to change in a predicted way. The stability
 301 of diamond detectors depends on many factors, e.g. material purity, polishing process,
 302 electrode material, irradiation damage etc. The aim is to study the behaviour of
 303 diamond under controlled conditions, with the goal to understand its limitations.
 304 One of these limitations is the received radiation dose as it can affect the long-term
 305 stability of the sensor during operation.

306 The three diamond samples (S37, S79 and S52) have been exposed to two different
307 types of ionising radiation for a longer period to see if their behaviour changes over
308 time. Two parameters have been observed in particular:

- 309 1. Charge collection of β particles and
310 2. Charge collection and ionisation profile of α particles.

311 **β long-term stability**

312 The diamond samples have undergone a long-term stability test at room temperature
313 using β radiation. This has been done using a ^{90}Sr source emitting ~ 2.28 MeV
314 electrons at a rate of approximately $10^4 \text{ e}^- \text{ cm}^{-2}$. To simulate the initial conditions in
315 HEP experiments, the sensors must not be primed before starting the measurements.
316 The measurement setup consists of a diamond sample (S37, S52 or S79) with the
317 CIVIDEC Cx spectroscopic amplifier, a silicon diode with a CIVIDEC C6 amplifier
318 for triggering and a ^{90}Sr source on top. A particle emitted by the source traverses the
319 sensor bulk and hits the silicon diode, triggering the analogue signal readout. The
320 source is left on the top for the course of the experiment. The measurements, however,
321 are taken at discrete times. For every data point, approximately 10^4 triggers have
322 to be recorded. The offline analysis of the recorded signal pulse amplitudes yields a
323 Landau distribution for every data point. The current charge collection relative to the
324 initial charge collection for every sample is plotted as a function of the received β dose
325 in figure 1.8. It shows that, for the irradiated samples, the charge collection efficiency
326 improves when the diamond sensor is primed with a β source. The effect is negligible
327 for the non-irradiated high-quality S37. Both relative increases are significant – 22 %
328 for S79 and 55 % for S52. At a received dose of approximately 4×10^6 particles the
329 charge collection is stabilised. At that point S79 achieves close to a full efficiency (in
330 absolute values – not shown) whereas S52 reaches approximately 50 %.

331 The ~ 2.28 MeV electrons emitted by this source are not MIPs; their charge depo-
332 sition is higher than that of an electron MIP, according to the Bethe-Bloch distribu-
333 tion [7]. Nevertheless, for the purpose of these measurements this energy is adequate
334 since only the relative change in charge collection is of interest.

335 To sum up, diamond provides a stable measurement of the β radiation detection
336 after reaching a stable state. Even if damaged by radiation, it reaches a stable charge
337 collection at a received dose of $\sim 4 \times 10^6$ MIPs. Its efficiency decreases with a high
338 irradiation dose. However, the decrease can be accounted for if the damage factor
339 and the rate and energy of the particles are known. γ radiation has a similar impact
340 on the diamond as the β . The incident photons, if they interact with the diamond,
341 prime the bulk, increasing the charge collection efficiency. The difference, however,
342 is that the interaction probability (cross-section) is lower for gammas [18, 10].

1.3. RADIATION LIMITATIONS

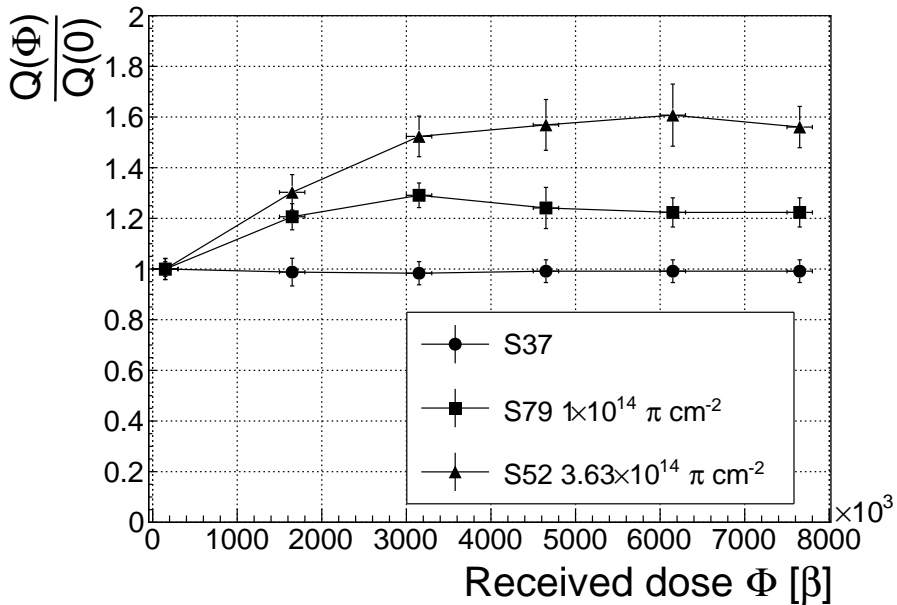


Figure 1.8: Relative increase of charge collection over time due to priming with the ^{90}Sr radioactive source. The charge collection for the non-irradiated S37 stays constant. The bias voltage for this measurement is 1 V/ μm .

343 **α long-term stability**

344 This part discusses the stability of irradiated diamond sensors during α measurements.
 345 An ^{241}Am source has been used, emitting α particles with a mean energy of 5.5 MeV.

346 To test the stability of the diamond during α measurements, the samples have
 347 been biased at +500 V and exposed to up to 8000 α hits while measuring their charge
 348 collection efficiency using the CIVIDEC Cx spectroscopic amplifier. The charge col-
 349 lected at every measurement point $Q(\Phi)$ is compared to collected charge of the first
 350 measurement $Q(0)$. The resulting ratio $\frac{Q(\Phi)}{Q(0)}$ for all samples is shown in figure 1.9.
 351 Each measurement point is an average of 30 consecutive α hits. The observations are
 352 the following:

- 353 - $Q(\Phi)$ for the non-irradiated S37 is stable as compared to $Q(0)$ over the course
 354 of the measurement.
- 355 - The initial efficiency of the irradiated S52 and S79 starts decreasing already at
 356 a low α count.
- 357 - The charge collection efficiency of the unprimed irradiated samples drops much
 358 faster than after priming.
- 359 - The particle count rate decreases with decreased efficiency, which is clearly seen
 360 in the unprimed S52 data where the data points at a low efficiency are much
 361 further apart.

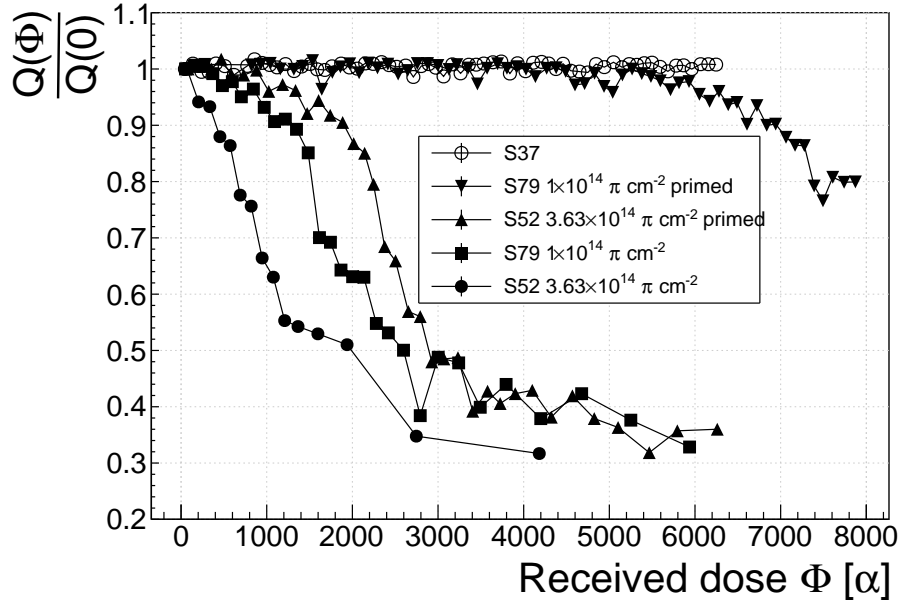


Figure 1.9: A relative drop in charge collection efficiency as a function of the received α dose for non-irradiated and irradiated diamond samples.

³⁶² The absolute values are not shown here because only the relative drop is of interest
³⁶³ in the scope of the long-term stability tests.

³⁶⁴ α affect the irradiated diamond differently than when subjected to β radiation.
³⁶⁵ This can be due to several contributions:

³⁶⁶ **Quantity of deposited energy.** The deposited energy on its path produces 24 times
³⁶⁷ more e-h pairs than that of a MIP, according to equations ?? and ???. Such a difference
³⁶⁸ may affect the charge collection efficiency due to saturation.

³⁶⁹ **A point-like charge carrier creation.** The energy of an α particle is deposited in
³⁷⁰ a small volume – 14 μm in depth and \sim 20 nm radially [13]. A dense distribution of
³⁷¹ charge carriers might affect their behaviour at the start of the drift.

³⁷² **Single-polarity charge carriers.** Carriers of only one polarity drift through the
³⁷³ sensor while those of the opposite polarity almost instantly reach the adjacent elec-
³⁷⁴ trode. Therefore the charges only one polarity get trapped along the drift path,
³⁷⁵ contributing to a single-polarity space-charge build-up.

³⁷⁶ To investigate this sudden drop in efficiency, the current pulse shapes using a
³⁷⁷ CIVIDEC C2 current amplifier have to be observed, as shown in figure 1.10. The
³⁷⁸ shape of the pulse holds more information about the charge carrier properties in the
³⁷⁹ sensor than solely the value of the integrated charge. This time only the primed S79
³⁸⁰ sample has been tested. Both the hole and the electron collection are observed to
³⁸¹ determine whether they behave differently or not.

1.3. RADIATION LIMITATIONS

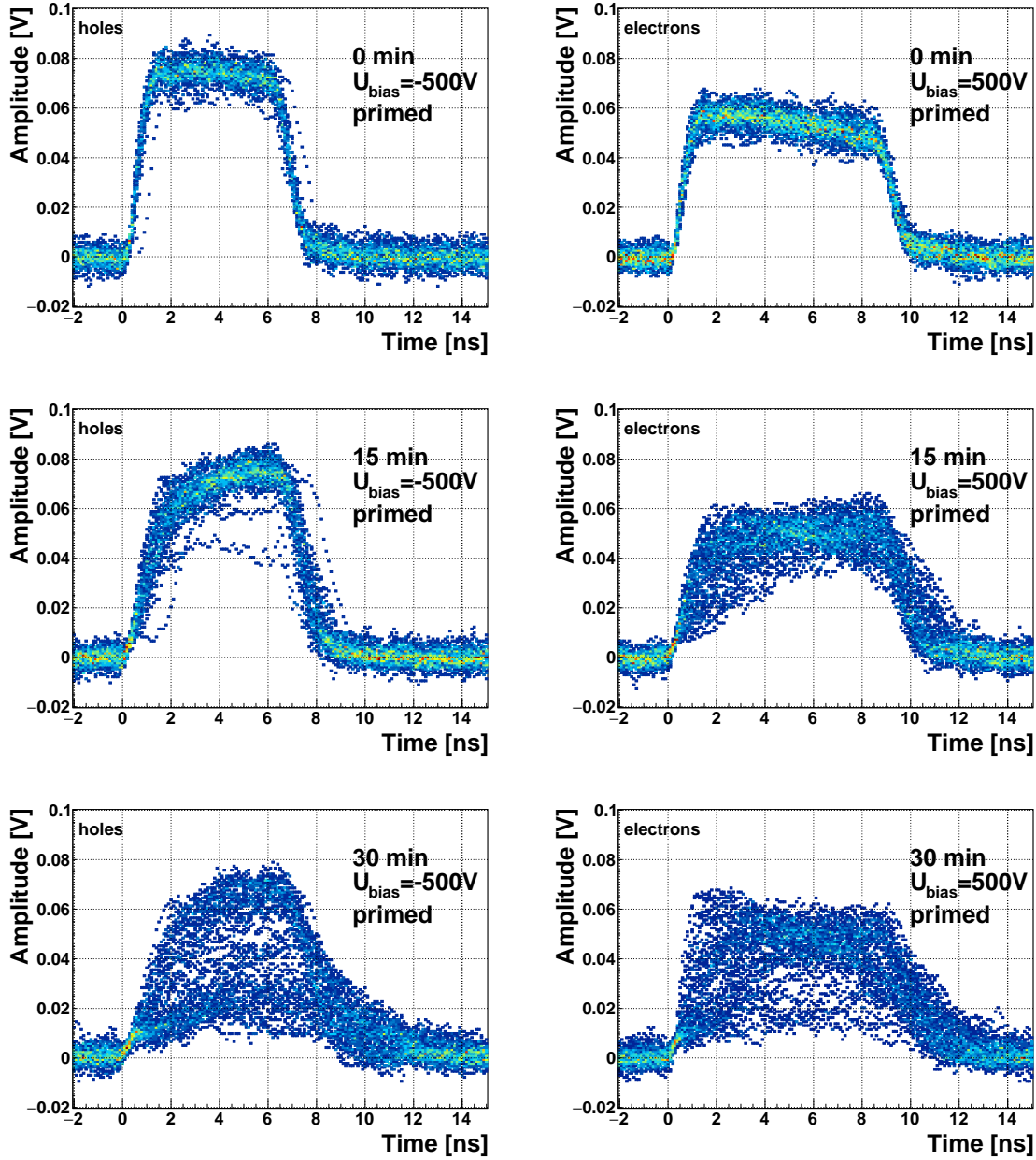


Figure 1.10: The signal of the irradiated and primed S79 deteriorates with time for both polarities. Every plot contains 60 superimposed pulses.

382 The first observation of the raw acquired data in figures 1.10 is that the initially
 383 stable pulses start deteriorating; several different shapes start appearing gradually,
 384 some still very similar to those from the beginning while the others with almost zero
 385 amplitude.

386 A more dedicated analysis of the first observation has been carried out as follows:
 387 at the beginning of the test when the diamond is still operating stably, 60 pulses are
 388 recorded. An average pulse is calculated. This is a reference pulse for the subsequent

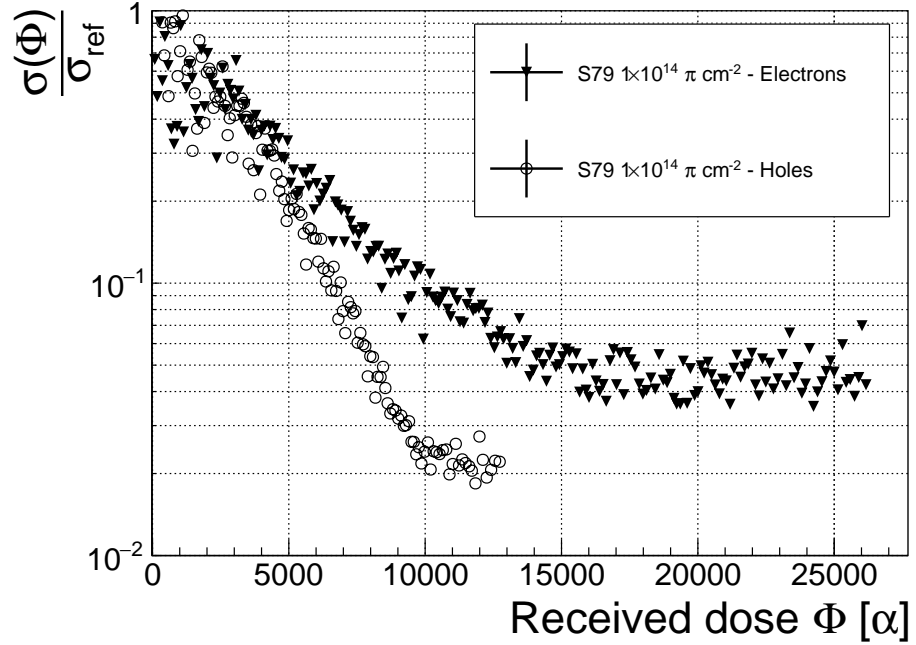


Figure 1.11: Deterioration of the pulse shapes with time.

measurement points. Then an RMS of the individual pulses σ_n with respect to the reference pulse is calculated and the resulting RMS values are summed together into σ_{ref} :

$$\sigma_{\text{ref}} = \sum_{n=1}^{60} \sigma_n. \quad (1.7)$$

All the subsequent data points also consist of a set of 60 pulses. At every data point the summation of the RMS values of the individual pulses with respect to the initial averaged pulse σ is calculated according to equation 1.7. The ratio between the initial σ_{ref} and discrete values σ gives a measure of the change of the pulse shape with respect to the reference pulse at the start of the measurement. Therefore the initial value is 1 and it decreases if the RMS values of subsequent data points are higher. Figure 1.11 shows the ratio $\frac{\sigma_{\text{ref}}}{\sigma(\alpha \text{ dose})}$. From the data obtained it can be concluded that the initial pulse shape quickly starts deteriorating. In fact, the deterioration of the shape follows an approximate exponential decay function, which can be fitted to the data. The resulting decay constants for electrons and holes are $\tau_e = (4400 \pm 150) \alpha^{-1}$ and $\tau_h = (3300 \pm 140) \alpha^{-1}$. The electrons retain the initial shape for longer. The deteriorated shapes also seem to be for a factor of 2 better than those of the holes.

Discussion One hypothesis is that this behaviour is caused by space-charge build-up. Charge carriers get stopped in the charge traps in the bulk for a long time, building up regions of space-charge. The built up space-charge affects the electric field. The field in turn affects the drifting charge carriers, slowing them down or speeding them

1.3. RADIATION LIMITATIONS

408 up, depending on the field gradient. Since the movement of the carriers is inducing
409 the electric current, the field gradient can be observed in the current signal.

410 The fact that the signal shapes vary significantly might be due to a very non-uniform
411 electric field, which is created by the three competing processes discussed above. The
412 charge carriers are created in a small volume whereby some immediately get trapped,
413 some recombine to form excitons ?? and others start drifting. The remaining charge
414 carriers drift towards their respective electrodes. Both are trapped on their way,
415 causing the space-charge build-up of one polarity on the first 14 μm and of the other
416 polarity all along the sensor thickness. A resulting electric field is very non-uniform,
417 which explains the unstable current pulses.

418 **Restoring the pulse shapes** Finally, an effort has been made to find a way for the
419 pulse shapes to return to their initial state. Five methods are listed:

- 420 1. No source, with bias voltage,
- 421 2. No source, without bias voltage,
- 422 3. Priming with γ at a rate of $400 \text{ s}^{-1}\text{cm}^{-1}$ without bias voltage,
- 423 4. Priming with β at a rate of $1000 \text{ s}^{-1}\text{cm}^{-1}$ with bias voltage and
- 424 5. Priming with β at a rate of $1000 \text{ s}^{-1}\text{cm}^{-1}$ without bias voltage.

425 Before starting each method, the diamond sample S79 is first primed using a ^{90}Sr
426 source for approximately one hour. Then the bias voltage is switched on and an
427 ^{241}Am source is put on top. The pulses produced by the incident α particles have a
428 proper rectangular pulse at the beginning, but then start changing – first gradually
429 and later increasingly more in an erratic way, as described in the text above. After
430 approximately 30 minutes, one of the methods is tested. When a “healing” procedure
431 is started, a set of 60 pulses is taken at irregular points of time to observe the change
432 in the pulse shape and to assess the quality of the “healing” procedure. Then the
433 bias voltage is switched off and the sample is primed again to reset its state before
434 starting with the next run.

435 The results depicted in figure 1.12 show that the methods (3) and (5) improve the
436 shape, method (2) helps slowly, (1) does not show any change with time and (4) at first
437 improves, but then significantly degrades the shape. The effect observed in method
438 (4) has already been described in [15]. The “healing” process therefore depends on
439 the rate of radiation, the bias voltage and the time of exposure. The ionising radiation
440 creates free charges, which quickly recombine close to the place of generation. It is
441 likely that they also release the charges trapped during the measurement, reducing the
442 overall effect of the space-charge. The traps get filled with both flavours of carriers,
443 thus they are neutralised. The pulse shape gradually returns to its initial state.

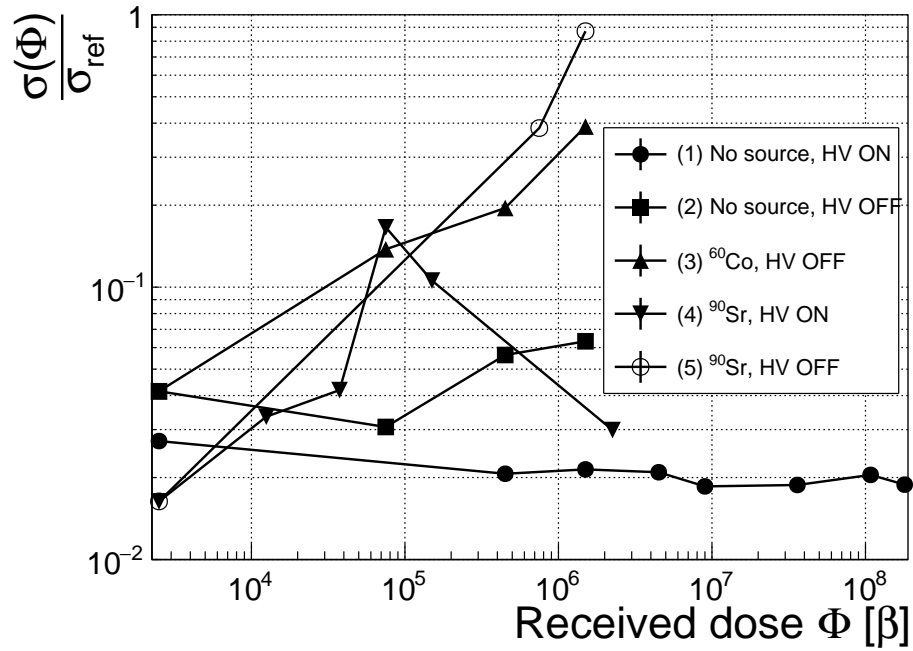


Figure 1.12: Comparison of the five procedures for the “healing” process for an irradiated diamond that had been exposed to α radiation with a rate of 10^1 s^{-1} , with the bias voltage switched on, for at least 30 minutes.

Procedure	Source	Type of radiation	Bias voltage	Effectiveness
1	/	/	ON	no
2	/	/	/	slow
3	^{60}Co	γ	/	YES
4	^{90}Sr	β	ON	no
5	^{90}Sr	β	/	YES

445

Table 1.2: Effectiveness of healing procedures.

446 **Summary** The shape of the pulses caused by α radiation changes with time for
 447 irradiated samples. The shape of the pulses gets distorted and becomes erratic. The
 448 charge collection decreases and its spread increases. The signal shapes are probably
 449 affected by a non-uniform electric field, which is caused by the build-up of space
 450 charge. The signal degradation happens even faster for non-primed diamonds. To
 451 “heal” the diamond – to bring the pulse shapes back to their initial shape – the
 452 sample must be primed using a β or a γ source for several minutes without bias
 453 voltage. Switching to the inverse polarity for a few seconds helps a bit, but in a long
 454 run distorts the signal, preventing it from returning to the initial shape.

1.4. TEMPERATURE LIMITATIONS

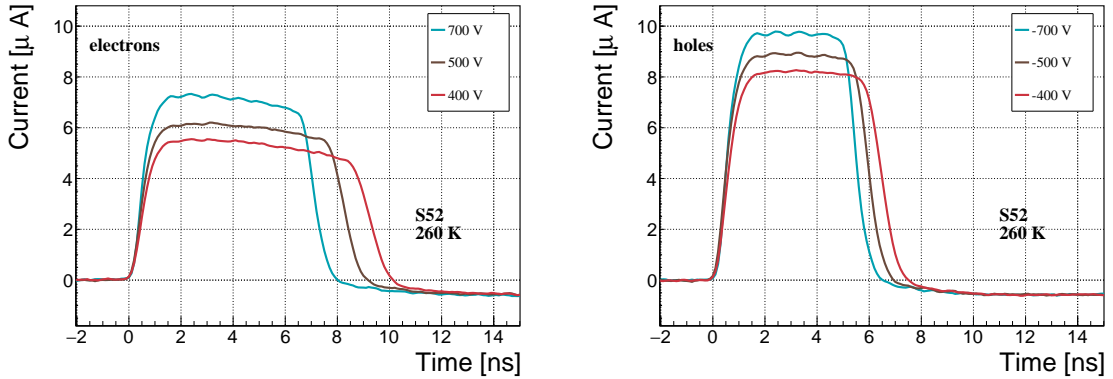


Figure 1.13: Varied bias voltage at a fixed temperature.

455 1.4 Temperature limitations

456 A test has been carried out to evaluate the effect of temperature changes on the
 457 output signal of the diamond sensors. A cryostat filled with liquid helium is used to
 458 cool down the sensor during the measurement process. The current signal response
 459 to α -particles is measured at 18 temperature points between 4 K and 295 K. At
 460 every temperature point a set of 300 pulses is recorded at various bias voltages. The
 461 resulting data show that the charge collection is stable from RT down to 150 K where
 462 it starts decreasing. It stabilises again at about one third of the initial value at 75 K.
 463 This behaviour was first measured and discussed by H. Jansen [13].

464 1.4.1 Temperature-variant α -TCT before irradiation

465 Three sCVD diamond samples have been tested at a range of temperatures using
 466 the α -TCT technique. At each temperature point, the bias voltage is set to several
 467 positive and negative values. A set of 300 pulses is recorded at every data point
 468 and averaged offline. The resulting averaged pulses of sample S37 at the 260 K
 469 temperature point and a bias voltage of ± 700 V, ± 500 V and ± 400 V are shown in
 470 figure 1.13. The pulses induced by holes as charge carriers are shorter than those
 471 induced by electrons, which means that holes travel faster in diamond. The area of
 472 the pulse, however, is the same for both polarities, which corresponds to the fact that
 473 the same amount of charges is drifting in both cases.

474 Figure 1.14 shows pulses at a bias voltage set to ± 500 V across the range of
 475 temperatures between 4 K and 295 K. Several conclusions can be drawn by observing
 476 their shape. First, the pulse shapes change with decreasing temperature. The pulse
 477 time gets shorter and higher, hinting at the faster carrier drift velocity v_{drift} . Second,
 478 between 150 K and 75 K there is a significant change in shape - the time constant of
 479 the rising edge increases significantly and the pulse area decreases. From 75 K down
 480 to 4 K there is no significant change. Last, the top of the pulse at the S52 is not flat,

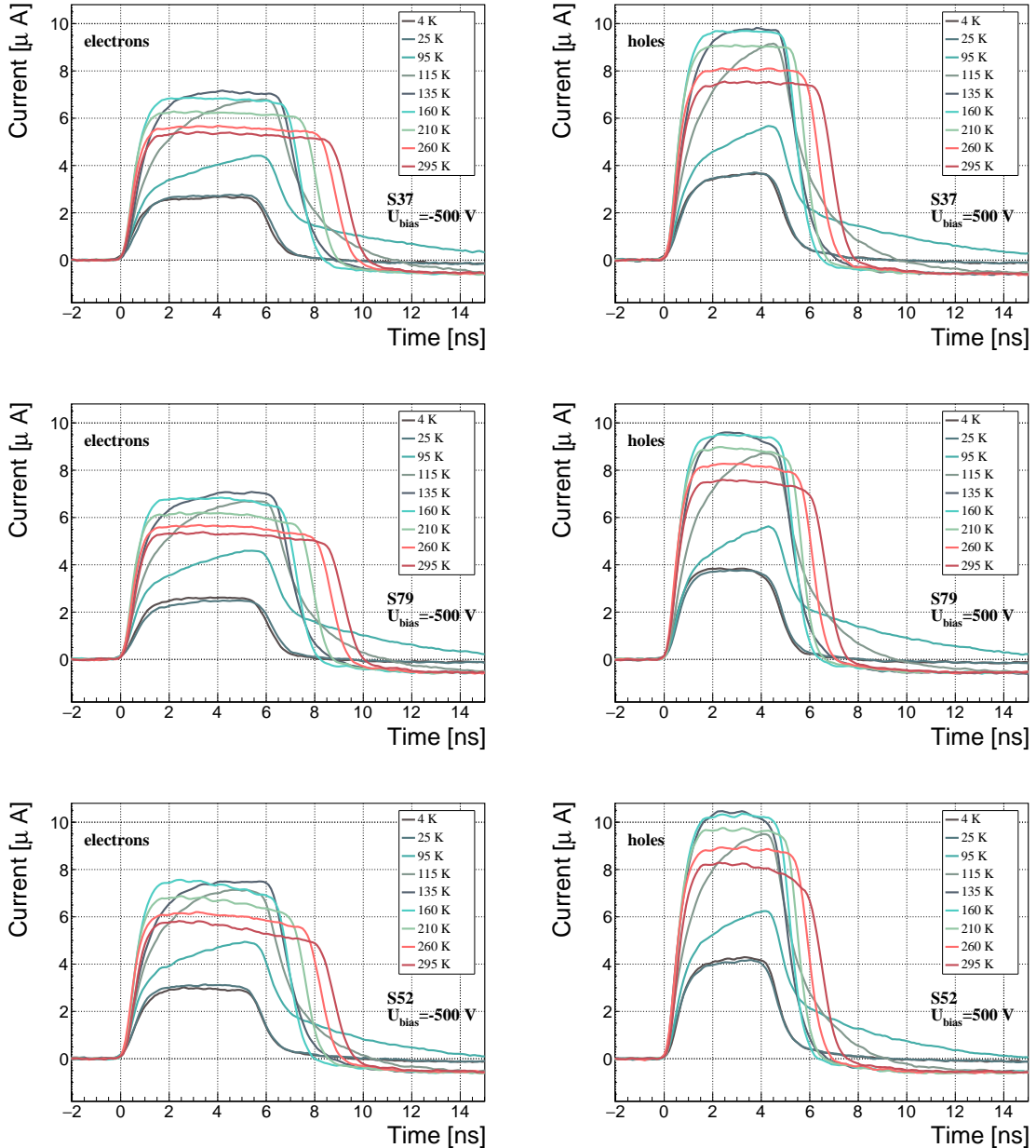


Figure 1.14: Several data points between 4 K and 295 K at a bias voltage of ± 500 V. The tilted top of the pulse on the bottom left figure is due to built-up space charge.

1.4. TEMPERATURE LIMITATIONS

⁴⁸¹ which means that a portion of the drifting charge is lost along the way. This is due
⁴⁸² to charge trapping, likely by means of crystal defects or impurities.

⁴⁸³ 1.4.2 Temperature-variant α -TCT after irradiation

⁴⁸⁴ The irradiated S79 and S52 have been re-tested in the cryostat after irradiation. The
⁴⁸⁵ aim is to observe how their pulse shapes change with decreasing temperature, in
⁴⁸⁶ particular the decaying top of the pulses, as shown in figure 1.15. The decay time
⁴⁸⁷ gives information on trapping of charge carriers while travelling through the diamond
⁴⁸⁸ bulk. A variation of the decay time constant as a function of temperature might
⁴⁸⁹ help to reveal the type and depth of the charge traps. To observe these effects or
⁴⁹⁰ lack thereof, a number of requirements have to be met. First, the diamond samples
⁴⁹¹ are intentionally not primed prior to the experiment because priming would improve
⁴⁹² the pulse shapes and possibly change the decay time constant of the signal. Second,
⁴⁹³ keeping in mind that the pulse shape of irradiated diamonds changes with time, the
⁴⁹⁴ duration of the measurement of an individual data point has to be short – of the
⁴⁹⁵ order of 30 seconds. Last, the sequence of the bias voltage settings is important, the
⁴⁹⁶ reason for which is explained below.

⁴⁹⁷ Unfortunately it is not possible to avoid temporal pulse changes. For instance,
⁴⁹⁸ one measurement point takes approximately one minute. After the measurement, the
⁴⁹⁹ bias voltage polarity is swapped for a few seconds to bring the diamond back into
⁵⁰⁰ its initial state. But a few seconds with respect to a minute are not enough, but
⁵⁰¹ due to time constraints this cannot be avoided. Therefore when the bias voltage is
⁵⁰² set to the next value, there is still some residual effect of the previous measurement.
⁵⁰³ Similar to the effects of polarisation, this effect is also decreasing the pulse height.
⁵⁰⁴ This can be observed in figure 1.15, which shows the resulting pulses of S52 for bias
⁵⁰⁵ voltages of ± 200 V, ± 300 V, ± 400 V and ± 500 V at 230 K and 260 K. In this case
⁵⁰⁶ the measurement sequence is: 230K (200 V, 300 V, 400 V, 500 V, -500 V, -400 V,
⁵⁰⁷ -300 V), 260 K (-200 V, -300 V, -400 V, -500 V, 500 V, 400 V, 300 V). The changes in
⁵⁰⁸ pulse shapes for holes at 230 K and 260 K cannot be attributed to the temperature
⁵⁰⁹ change. Instead, the explanation could lie in diamond “polarisation”. This means
⁵¹⁰ that, when exposed to an electric field with α measurements ongoing, an internal
⁵¹¹ electric field of inverse polarity builds up in the diamond, which effectively reduces
⁵¹² the overall electric field. This internal field does not dissipate when the external
⁵¹³ bias voltage is switched off. The diamond becomes “polarised”. When switching the
⁵¹⁴ polarity of the external bias voltage, the internal and external electric field point in
⁵¹⁵ the same direction at the beginning, increasing the overall electric field and with it
⁵¹⁶ the pulse height. In figure 1.15 this happens when switching from 500 V (figure 1.15a)
⁵¹⁷ to -500 V (figure 1.15b) at 230 K. The built up polarisation contributes to the pulse
⁵¹⁸ having a sharp rising edge and a high amplitude. This effect decays during the next
⁵¹⁹ two voltage points. There would be a handful of ways to avoid this polarisation effect
⁵²⁰ in the data:

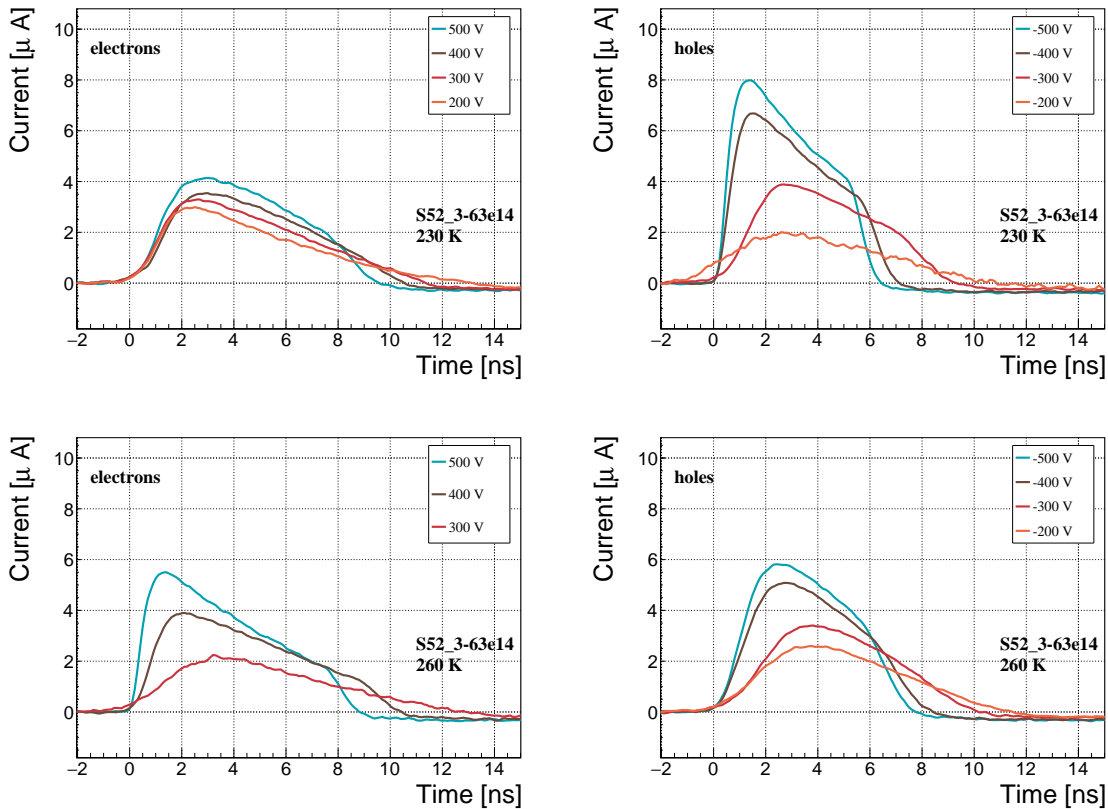


Figure 1.15: Varied bias voltage at a fixed temperature for an irradiated sample.

- 521 1. After every data point invert the bias voltage and leave it to return to a neutral
- 522 state for the same amount of time,
- 523 2. Make a hysteresis of data points, going from minimum negative to maximum
- 524 positive bias several times,
- 525 3. Reduce the measurement time at every bias voltage setting.

- 526 Unfortunately, options (1) and (2) are very time consuming and would increase the
- 527 overall experiment time to over one day. The third option would worsen the resulting
- 528 averaged pulses. In the end an alternative option has been chosen: alternating the
- 529 starting bias voltage and the sequence at every temperature point. With this option,
- 530 a meaningful systematic error in analysing the pulse shapes can be attained.

531 Figure 1.16 shows the irradiated S52 and S79 as well as the non-irradiated S37
 532 for comparison, all at a bias voltage of ± 500 V and at several temperature points
 533 between 4 K and 295 K. It is evident that the radiation damage affects the shape of
 534 the pulses across all temperatures.

1.4. TEMPERATURE LIMITATIONS

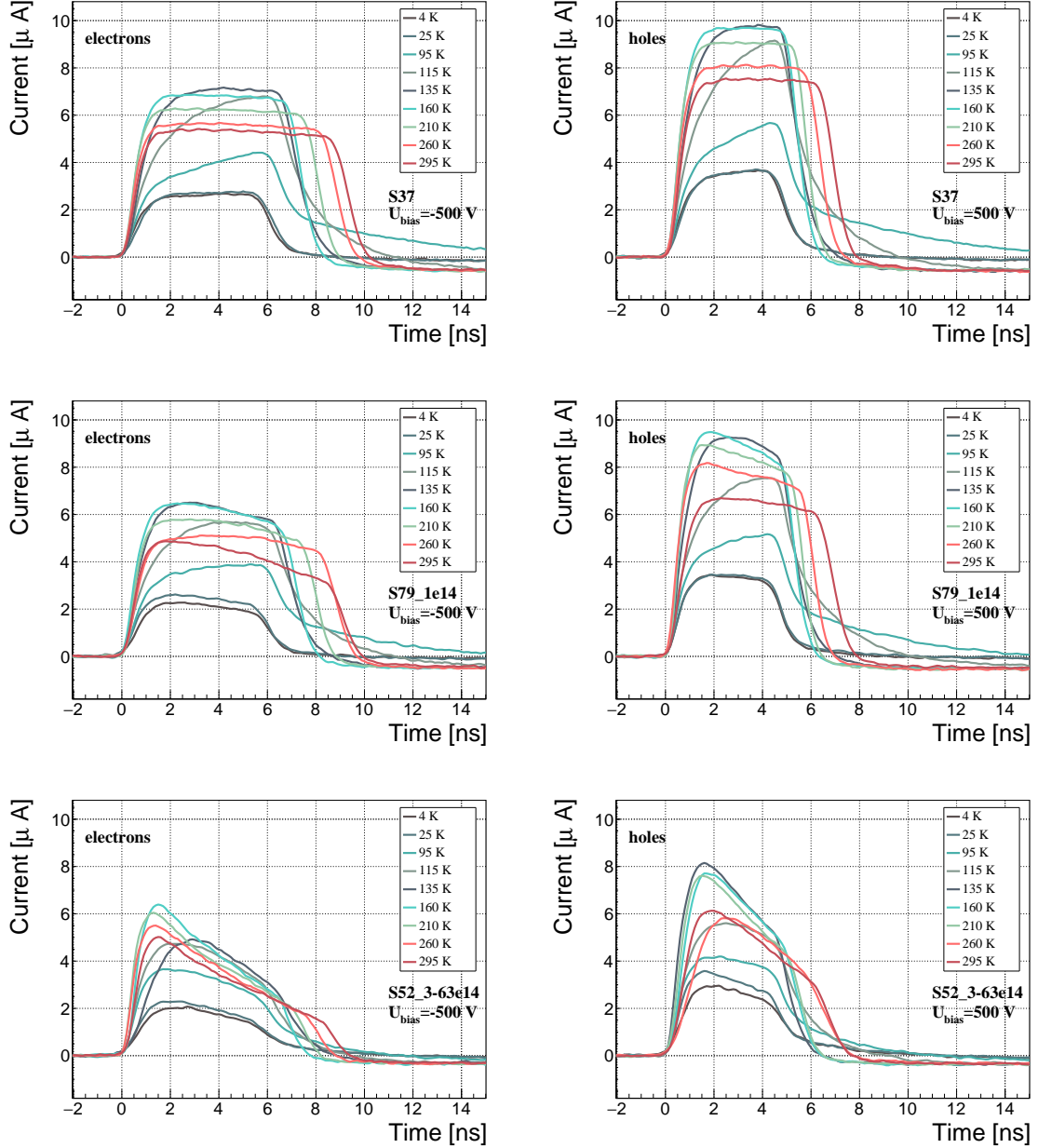


Figure 1.16: After irradiation: several data points between 4 K and 295 K at a bias voltage of ± 500 V.

535 Collected charge as a function of temperature

536 The collected charge as a function of temperature for electrons and holes is plotted
 537 in figures 1.17 and 1.18, respectively. In the framework of this thesis the focus is
 538 on the effect in the irradiated devices. The new contribution are the data points for
 539 the irradiated samples. The focus is on the temperature range between 4–75 K and
 540 150–295 K whereby the effect of the re-excitation of bound electrons and holes is not

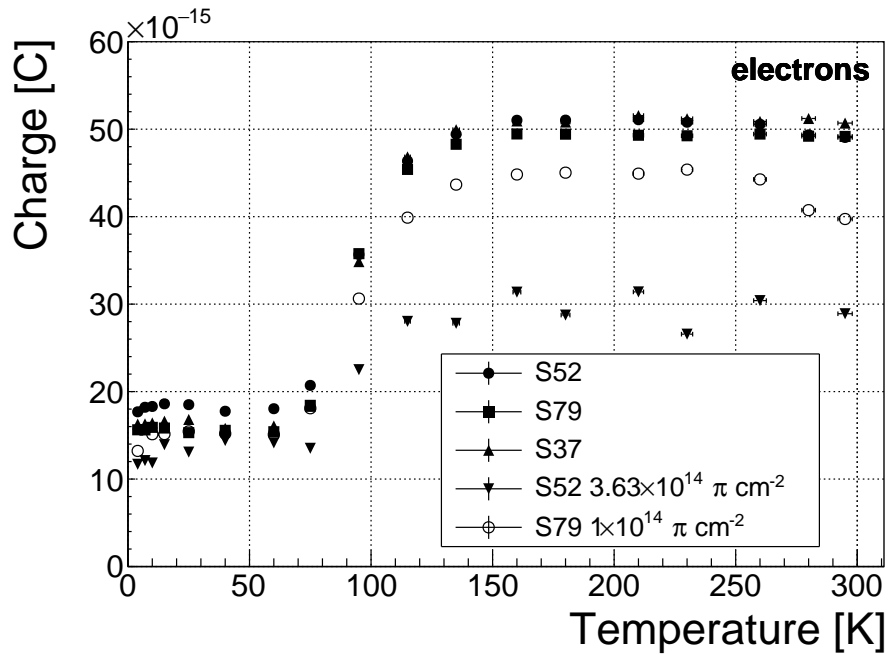


Figure 1.17: Collected charge for electrons as a function of temperature.

541 prevailing. The values for all samples are fairly stable in the range between 4 K and
 542 75 K and between 150 K and 295 K. However, in the values for the irradiated S52
 543 some excursions can be observed. This is due to the sequence of the measurement
 544 steps, which results in a hysteresis effect explained in the preceding text.

545 The collected charge drops significantly from 150 K down to 75 K. In the non-
 546 irradiated samples the values in the lower temperature range are approximately 30 %
 547 of those in the high range. For the irradiated samples this difference is lower: 35 %
 548 for S79 and 50 % for S52.

549 An interesting detail in figure 1.17 is that the ratio between the values for non-
 550 irradiated samples and their irradiated counterparts at the lower temperature range
 551 is different than at the higher range. In other words, the charge loss due to irradiation
 552 damage is lower for temperatures between 4 K and 75 K than for temperatures between
 553 150 K and 295 K. The irradiated S52 collects 78 % of the initial charge in the low
 554 temperature range, but only 59 % of the initial charge for the high range. The values
 555 for S79 for these two temperature ranges are 100 % and 90 %, meaning that the drop
 556 in charge collection efficiency after irradiation to $1 \times 10^{14} \pi \text{ cm}^{-2}$ is negligible for
 557 temperatures below 75 K.

558 Charge trapping

559 A decaying exponential function from equation ?? has been fitted to the decaying top
 560 of the averaged pulses at a bias voltages of $\pm 400 \text{ V}$ and $\pm 500 \text{ V}$ across all temperatures
 561 excluding the transitional range between 75 K and 150 K. The resulting decay time

1.4. TEMPERATURE LIMITATIONS

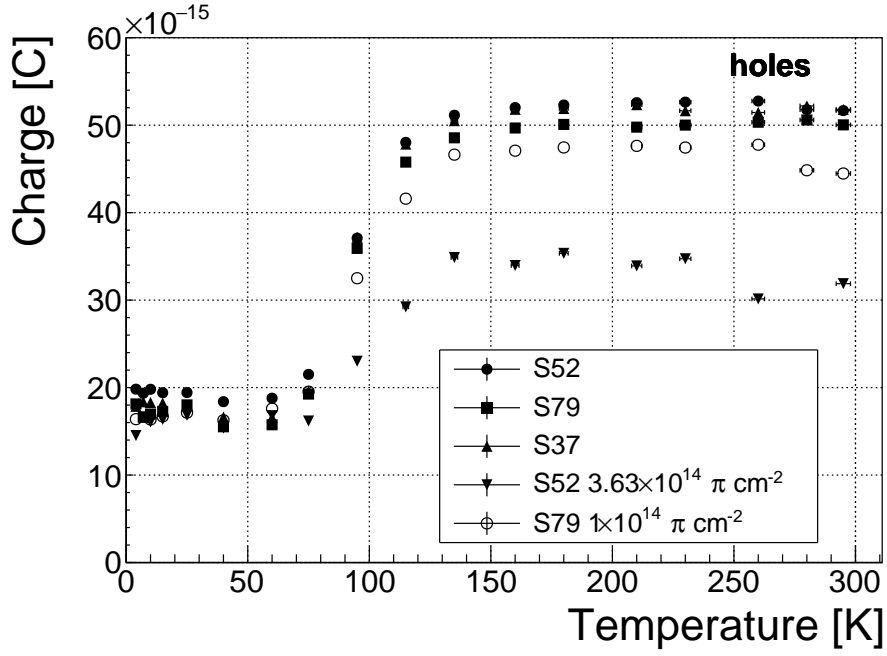


Figure 1.18: Collected charge for holes as a function of temperature.

constants τ for an individual temperature point are not equal, which stems from the fact that the pulses change with time due to “polarisation”. This counts as a systematic error. Therefore the fitted τ for ± 400 V and ± 500 V are averaged into one value representing the measurement at that temperature point. Figure 1.19 shows the fitted τ for the five samples between 4 K and 295 K. In principle the time constants should be infinite for an ideal and non-irradiated sample. Here a slightly tilted top of the pulse due to space-charge is already successfully fitted with an exponential function (a pitfall in the automatic analysis), resulting in a τ of the order of $(200 \pm 20) \times 10^{-9}$ s. Consequently the fitting method is not adequate for non-irradiated samples.

For the irradiated samples the fit becomes increasingly more meaningful. As seen in figure 1.19, the fitted values of the irradiated samples are fairly stable across all temperatures. There is a slight increase in the decay time constant of the S52 from $(6.0 \pm 0.5) \times 10^{-9}$ s above 150 K to $(8.5 \pm 0.9) \times 10^{-9}$ s below 75 K. On the other hand, this step is not observable in the S79 data. With only one sample exhibiting this behaviour, the effect is not significant enough. Judging by the data acquired, the samples would need to be irradiated to doses above $1 \times 10^{14} \pi \text{ cm}^{-2}$ to quantify this effect in detail. So far this effect is not regarded as significant for the scope of this thesis. Building on this assumption, the conclusion is that the signal decay time constant for irradiated sCVD diamond is constant across the temperature range between 4 K and 295 K, excluding the transitional range between 75 K and 150 K where it cannot be quantified properly.

Considering the discussion above, all the values can be averaged into one decay

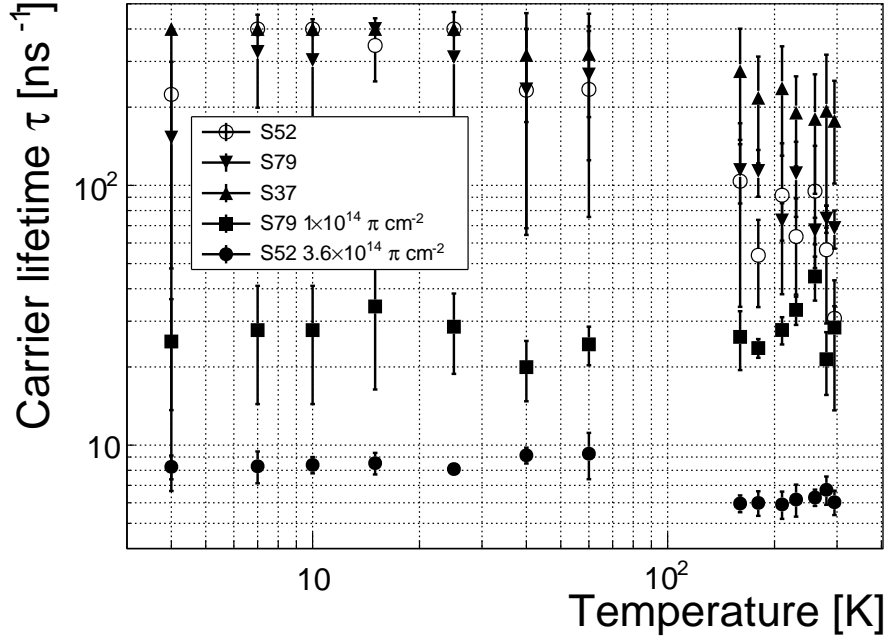


Figure 1.19: This figure shows the charge carrier lifetime as a function of temperature. The data points between 75 K and 150 K are omitted. The fit function only works well on signals with a well pronounced decaying top.

constant. Figure 1.20 shows these values for all samples as a function of the received $\pi_{300 \text{ MeV}}$ radiation dose. To estimate the charge carrier lifetime with respect to the radiation dose received, a similar model is used than that in section 1.5. This model states that the charge carrier lifetime is linearly decreasing with increasing radiation dose:

$$\frac{1}{\tau} = \frac{1}{\tau_0} + \kappa_\tau \cdot \Phi \quad (1.8)$$

$$\tau = \frac{\tau_0}{\kappa_\tau \tau_0 \Phi + 1} \quad (1.9)$$

where τ_0 is the lifetime for a non-irradiated sample (real lifetime, therefore of the order of 400 ns), τ is the lifetime of an irradiated sample, Φ is the received radiation dose and κ_τ the lifetime degradation factor. For these data the fitted factor is equal to $\kappa_\tau = (3.5 \pm 0.8) \times 10^{-16} \text{ s cm}^2 \pi_{300 \text{ MeV}}^{-1}$. Using this factor, the steepness of the decay in the pulse shape as a function radiation dose can be estimated. This is highly useful information when designing a system where the current pulse shape is an important factor.

1.5 Conclusion

This chapter gives an overview of the capabilities and limitations of diamond as a particle detector. Two effects on diamond are studied – radiation and temperature.

1.5. CONCLUSION

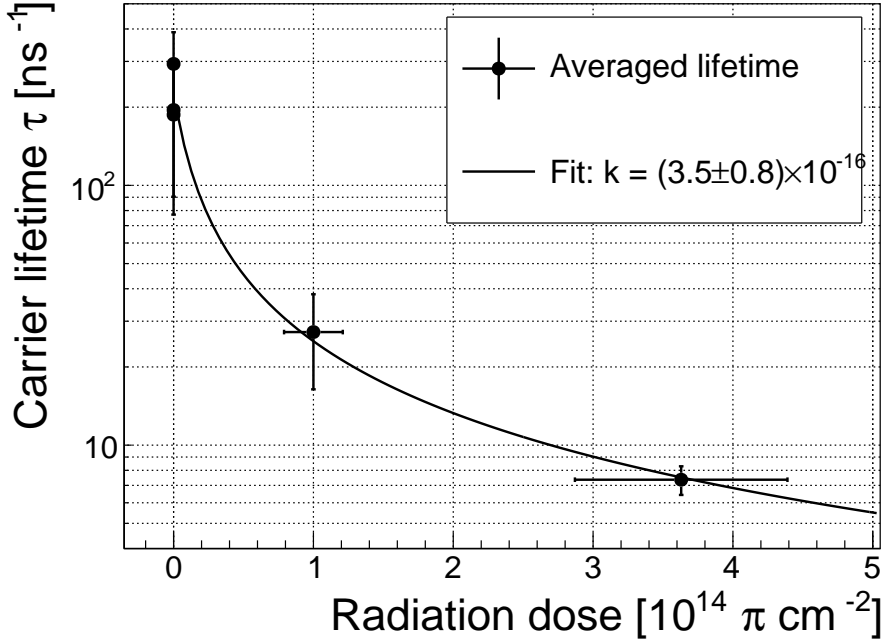


Figure 1.20: This figure shows the carrier lifetime averaged over all temperatures and plotted as a function of the π irradiation dose.

Two sCVD diamond detectors were irradiated with 300 MeV pions. They were tested alongside a non-irradiated sample to observe the changes in the ability to detect α , β and γ radiation. Their charge collection efficiency was measured in a test beam facility. The results were compared to the results from the RD42 collaboration and a DPA model. A radiation damage factor $k_\lambda = (4.4 \pm 1.2) \times 10^{-18} \mu\text{m}^{-1} \text{ cm}^{-2}$ was obtained for $\pi_{300 \text{ MeV}}$ particles. The data point was not in agreement with the data provided by RD42 nor with the model. However, the irradiation process and the low number of tested samples hold a relatively high statistical uncertainty. In addition, there was no diamond surface treatment done in between the measurements, as is the case in the study conducted by RD42. The results obtained in the course of these measurements are going to be fed into the existing pool of data in the RD42 collaboration.

The next step was to test the long-term capabilities for α detection. The shape of the ionisation profile was investigated to determine the behaviour of the charge carriers in the irradiated diamond. An exponential decay was observed in the pulses of irradiated samples, proving that there are charge traps in the bulk that were created during irradiation. Then a long-term stability test was carried out. The results show that the irradiated diamond detectors do not provide a stable and reliable long-term measurement of α particles. This might be due to a space-charge build-up in the bulk, which changes the electric field, affecting the charge carriers. A procedure to improve the pulse shape using β and γ radiation was proposed.

Finally, the diamond sensors were cooled down to temperatures between 4 K and

623 295 K. Their response to α particles was observed. The results of the non-irradiated
624 and irradiated samples were compared. The effect of reduction for the number of
625 drifting charges due to exciton recombination was observed in both sets of data.
626 The second set had a superimposed effect of charge trapping during the drift, which
627 was represented by an exponential decay in the signal. The decay time constant
628 did not change with temperature. Therefore all temperature points for individual
629 samples were averaged and the decay time constants were plotted against the received
630 radiation dose. A lifetime degradation factor $\kappa_\tau = (3.5 \pm 0.8) \times 10^{-16} \text{ s cm}^2 \pi_{300 \text{ MeV}}^{-1}$
631 for non-primed diamonds was defined.

⁶³² Bibliography

- ⁶³³ [1] *DRS4*. <https://www.psi.ch/drs/evaluation-board>.
- ⁶³⁴ [2] *Element Six*. <http://www.e6.com>.
- ⁶³⁵ [3] *IHa Technologies Pte. Ltd.* <https://www.2atechnologies.com>.
- ⁶³⁶ [4] *Paul Scherrer Institute*. <https://www.psi.ch/>.
- ⁶³⁷ [5] *RD42 collaboration*. <http://rd42.web.cern.ch/rd42/>.
- ⁶³⁸ [6] *Determination of operational dose equivalent quantities for neutrons*. ICRU,
⁶³⁹ Washington, DC, 2001.
- ⁶⁴⁰ [7] H. Bethe and J. Ashkin. *Experimental Nuclear Physics*, ed. E. Segre, page 253,
⁶⁴¹ 1953.
- ⁶⁴² [8] Giorgio Brianti. SPS North Experimental Area. Technical Report CERN-SPSC-
⁶⁴³ T-73-8. LabII-EA-Note-73-4, CERN, Geneva, 1973.
- ⁶⁴⁴ [9] P. Carazzetti and H. R. Shea. *Electrical breakdown at low pressure for planar
645 microelectromechanical systems with 10- to 500 μm gaps*. *J. Micro/Nanolith.
646 MEMS MOEMS*, (8(3), 031305), Jul-Sep 2009.
- ⁶⁴⁷ [10] E. Griesmayer and B. Dehning. Diamonds for beam instrumentation. *Physics
648 Procedia*, 37:1997 – 2004, 2012. Proceedings of the 2nd International Conference
649 on Technology and Instrumentation in Particle Physics (TIPP 2011).
- ⁶⁵⁰ [11] Moritz Guthoff, Wim de Boer, and Steffen Mller. Simulation of beam induced
651 lattice defects of diamond detectors using {FLUKA}. *Nuclear Instruments and
652 Methods in Physics Research Section A: Accelerators, Spectrometers, Detectors
653 and Associated Equipment*, 735:223 – 228, 2014.
- ⁶⁵⁴ [12] M. Huhtinen. Simulation of non-ionising energy loss and defect formation in
655 silicon. *Nuclear Instruments and Methods in Physics Research A*, 491:194–215,
656 September 2002.

BIBLIOGRAPHY

- 657 [13] Hendrik Jansen, Norbert Wermes, and Heinz Pernegger. *Chemical Vapour De-*
658 *position Diamond - Charge Carrier Movement at Low Temperatures and Use in*
659 *Time-Critical Applications.* PhD thesis, Bonn U., Sep 2013. Presented 10 Dec
660 2013.
- 661 [14] Claude A. Klein. Radiation-induced energy levels in silicon. *Journal of Applied*
662 *Physics*, 30(8):1222–1231, 1959.
- 663 [15] Gregor Kramberger, V. Cindro, A. Gorisek, I. Mandic, M. Mikuz, and M. Zavr-
664 tanik. Effects of bias voltage during priming on operation of diamond detectors.
665 *PoS*, Vertex2012:013, 2013.
- 666 [16] W. Y. Liang. Excitons. *Physics Education*, 5:226–228, July 1970.
- 667 [17] M. Mikuž. *Diamond sensors for high energy radiation and particle detection.*
668 TIPP, 2011.
- 669 [18] V. Sarin. *Comprehensive Hard Materials.* Elsevier Science, 2014. p. 411.
- 670 [19] M. Červ, P. Sarin, H. Pernegger, P. Vageeswaran, and E. Griesmayer. Diamond
671 detector for beam profile monitoring in comet experiment at j-parc. *Journal of*
672 *Instrumentation*, 10(06):C06016, 2015.
- 673 [20] J. L. Yarnell, J. L. Warren, and R. G. Wenzel. Lattice vibrations in diamond.
674 *Phys. Rev. Lett.*, 13:13–15, Jul 1964.